A Computationally Efficient Full-Speed Domain Control Method for PMaSynRM Considering Magnetic Saturation

Kaiwen Tan, Jianyong Su, *Member, IEEE*, Bencheng Zhong, and Guijie Yang

***Abstract*—The permanent magnet-assisted synchronous reluctance motor (PMaSynRM) has a wide speed range. Accurately resolving the optimal current operation point across the full-speed domain is crucial to ensuring the motor's efficient and reliable operation. Due to the partial neglect of the magnetic saturation characteristics in PMaSynRM, the operating point obtained by existing methods is suboptimal. This article presents a set of full-speed domain control methods. First, this article proposes maximum torque per ampere (MTPA) and maximum torque per voltage (MTPV) criteria that consider the partial derivative term of the inductance with respect to current, which has been ignored in previous methods. Furthermore, an initial iteration point optimization technique is proposed to reduce the increased computational burden resulting from more complex criteria, ensuring the algorithm's real-time implementation. The proposed method realizes an accurate and real-time solution of the optimal operating point. Compared to traditional methods, the proposed method has a higher torque enhancement in the MTPA region and a higher MTPV critical speed. The effectiveness of the proposed method is experimentally verified in a 5.5 kW PMaSynRM.**

***Index Terms*—Full-speed domain control, magnetic saturation, maximum torque per ampere (MTPA), maximum torque per voltage (MTPV), permanent magnet-assisted synchronous reluctance motors (PMaSynRM).**

I. Introduction

PERMANENT magnet-assisted synchronous reluctance motor (PMaSynRM) has gained much attention in the fields of industry and electric vehicles due to the advantages of high efficiency, high power density, high power factor, and wide speed range [1], [2]. The optimal control objectives are different in different speed regions for PMaSynRM. To improve the motor performance across a wide speed range, an optimal current control method based on the speed region is required.

The optimal current control methods can be categorized into model-free and model-based methods. The model-free methods do not require prior knowledge of motor parameters, such as injection-based methods [3], [4], search-based methods [5], [6], and feedback-based methods [7], [8]. Nevertheless, the restricted speed range and suboptimal dynamic performance of model-free methods make it challenging to meet the requirements of full-speed domain control. The model-based methods require obtaining motor parameters a priori and calculating the trajectory curves, which include the maximum torque per ampere (MTPA) curve, the maximum torque per voltage (MTPV) curve, the current limit (CL) curve, the voltage limit (VL) curve, and the constant torque curve [9], [10], [11], [12]. The essence of the model-based approach is to identify the only intersection point of the two curves at which the operating point resides. The underlying principles of these approaches are consistent across different speed regions, facilitating seamless transitions between different speed regions. Moreover, the model-based methods can directly determine the coordinates of the optimal operating point based on the motor's real-time speed and reference torque, enhancing the control system's dynamic performance. In summary, the model-based approaches, distinguished by their superior dynamic performance and adaptability across a wide range of speed domains, are suitable for the full-speed range control of PMaSynRM.

The full-speed control methods rely on the accurate MTPA and MTPV criteria. In [5], [13], and [14], the MTPA and MTPV criteria were derived without considering the variation of inductance with current. Unfortunately, both criteria significantly deviate from the optimal criteria when applied to synchronous motors with saturation characteristics [15], [16]. In [9] and [11], the significant variation of the inductance with current of the interior permanent magnet synchronous motor (IPMSM) was noticed, the dq-axis inductances were modeled as functions of the dq-axis currents, and the MTPA and MTPV criteria considering the variation of the inductance with current were derived. However, this approach still neglected the partial derivative of the inductance with respect to current. In [17], finite element analysis was carried out on an IPMSM with a rated power of 25 kW, and the results showed that the optimal MTPA criterion has a maximum torque improvement of 3.6% compared to the MTPA criterion that neglects the partial derivative of the inductance with respect to current. In [12], the partial derivative of the inductance with respect to current was considered only in the MTPA criterion; the proposed full-speed domain algorithm had to be operated at a reduced frequency (4 kHz) due to the increased computation burden. For IPMSM, the MTPA and

Received 20 August 2024; revised 19 December 2024; accepted 21 January 2025. Date of publication 27 January 2025; date of current version 20 March 2025. Recommended for publication by Associate Editor R. Kennel. *(Corresponding author: Jianyong Su.)*

The authors are with the School of Electrical Engineering and Automation, Harbin Institute of Technology, Harbin 150001, China (e-mail: 21B906033@stu.hit.edu.cn; sujianyong@hit.edu.cn; 18B906031@stu.hit.edu.cn; yangguijie@hit.edu.cn).

Color versions of one or more figures in this article are available at https://doi.org/10.1109/TPEL.2025.3535098.

Digital Object Identifier 10.1109/TPEL.2025.3535098

MTPV criteria, which consider the partial derivative of the inductance with respect to current, have yet to be applied in real-time control systems due to the significant increase in computational cost and slight performance improvement [9], [11]. PMaSynRM has more significant magnetic saturation characteristics than IPMSM due to its primary dependence on the reluctance torque rather than the permanent magnet torque [18]. Unfortunately, the existing MTPA and MTPV criteria for optimal current control in PMaSynRM ignore the partial derivative of the inductance with respect to current [10], [19]. Thus, exploring the implications of magnetic saturation in PMaSynRM becomes particularly relevant, especially focusing on the partial derivative of the inductance with respect to current in the context of refining the MTPA and MTPV criteria.

The full-speed domain control methods require real-time calculation of the intersection of two specific trajectory curves, which is accomplished by a numerical solution algorithm [9], [10], [11], [12], [20]. Specifically, in [11], the iterative computation time of Newton–Raphson (N–R), Levenberg–Marquardt, and gradient descent in different operation intersection cases were discussed, and the results showed that the N–R iterative algorithm has the highest computational efficiency. The convergence speed of N–R iteration is related to the initial point selection. A reasonable selection of the initial point can reduce the iteration times and ensure iterative stability [9], [10], [11]. Unfortunately, the selection of initial iteration points in the full-speed domain control process is arbitrary. Therefore, proposing an initial iteration point optimization technique (IIPOT) at each N–R iteration calculation for full-speed domain control is of great significance.

In this article, a computationally efficient full-speed domain control method for PMaSynRM that considers magnetic saturation is proposed. The main contributions are given as follows.

1) The proposed MTPA and MTPV criteria consider the partial derivative of the inductance with respect to current of PMaSynRM, which is more accurate.
2) The proposed IIPOT effectively reduce the iteration times for intersection computation, which ensures the algorithm's real-time implementation.
3) The proposed full-speed domain control method has a higher torque enhancement in the MTPA region and a higher MTPV critical speed.

The rest of this article is organized as follows. Section II provides the analysis of conventional full-speed domain control. In Section III, an improved full-speed domain control method is proposed. Experimental results are shown in Section IV. Finally, Section V concludes this article.

II. Analysis of Conventional Full-Speed Domain Control

A. PMaSynRM Model

The voltage equations of PMaSynRM in the dq reference frame are described as follows:

$$u_d = R_s i_d + \frac{\partial \psi_d (i_d, i_q)}{\partial t} - \omega_e \psi_q (i_d, i_q)$$

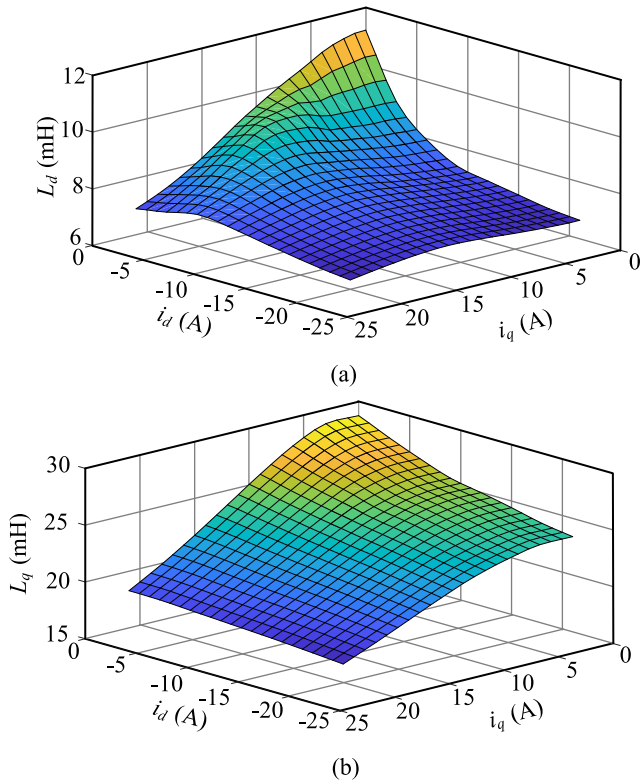

Fig. 1. dq-axis inductance maps for the PMaSynRM. (a) d-axis. (b) q-axis.

$$u_q = R_s i_q + \frac{\partial \psi_q (i_d, i_q)}{\partial t} + \omega_e \psi_d (i_d, i_q) \tag{1}$$

where u_d, u_q are the stator voltages; i_d, i_q are the stator currents, ψ_d, ψ_q are the flux linkages; R_s and ω_e represent the stator resistance and electrical speed, respectively. ψ_d, ψ_q can be described

$$\begin{cases} \psi_d (i_d, i_q) = L_d (i_d, i_q) \cdot i_d + \psi_f \\ \psi_q (i_d, i_q) = L_q (i_d, i_q) \cdot i_q \end{cases} \tag{2}$$

where L_d and L_q are dq-axis apparent inductances, respectively, and these are regarded as functions of the dq-axis currents. Fig. 1 shows the dq-axis inductance maps of the PMaSynRM, obtained through the experimental method introduced in [21].

The torque equation of PMaSynRM is described as

$$T_e = \frac{3}{2} P_n \left[\psi_d (i_d, i_q) \cdot i_q - \psi_q (i_d, i_q) \cdot i_d \right]. \tag{3}$$

B. Conventional MTPA and MTPV Criteria

The MTPA criterion is to achieve the reference torque by minimizing the total stator current. When the variation of inductance with current is ignored (i.e., regarding the inductance as a constant), the MTPA criterion can be briefly expressed [9], [10], [13], as

$$i_d = \frac{-\psi_f + \sqrt{4 (L_d - L_q)^2 i_q^2 + \psi_f^2}}{2 (L_d - L_q)}. \tag{4}$$

The error of the abovementioned criterion is discussed, and an MTPA criterion that considers magnetic saturation

is proposed, as shown in (5). However, this criterion ignores the partial derivative of the inductance with respect to current [9], [11], [22]

$$\left(L_d\left(i_d,i_q\right)-L_q\left(i_d,i_q\right)\right)\left(i_d^2-i_q^2\right)+\psi_f i_d=0. \tag{5}$$

The MTPV criterion is to minimize the stator voltage while achieving a reference torque. Similar to the MTPA criterion, the MTPV criterion has the same development based on the consideration of magnetic saturation. The conventional MTPV criterion ignoring the variation of inductance with current is given as follows [23], [24], [25]:

$$i_d=-\frac{\psi_f}{L_d}+\frac{-L_q\psi_f+\sqrt{L_q^2\psi_f^2+4\left(L_d-L_q\right)^2L_q^2i_q^2}}{2L_d\left(L_d-L_q\right)}. \tag{6}$$

MTPV criterion that ignores the partial derivatives of the inductance with respect to current [9], [11], [12]

$$L_d\left(i_d,i_q\right)i_d^2+L_q\left(i_d,i_q\right)i_q^2+\psi_f i_d-\frac{L_q^2\left(i_d,i_q\right)i_q^2}{L_d\left(i_d,i_q\right)}-\frac{\left(L_d\left(i_d,i_q\right)i_d+\psi_f\right)^2}{L_q\left(i_d,i_q\right)}=0. \tag{7}$$

C. Solving the Intersection

The system of equations for the intersection point is described as

$$\begin{cases}f_1\left(i_d^*,i_q^*\right)=0\\ f_2\left(i_d^*,i_q^*\right)=0\end{cases} \tag{8}$$

where f_1 and f_2 are the two trajectory curves on which the intersection lies. The N–R iterative method is used to solve this nonlinear problem. The general iterative form is as follows:

$$\begin{bmatrix}i_d^*(k+1)\\ i_q^*(k+1)\end{bmatrix}=-\mathbf{J}(k)^{-1}\begin{bmatrix}f_1\left(i_d^*(k),i_q^*(k)\right)\\ f_2\left(i_d^*(k),i_q^*(k)\right)\end{bmatrix}+\begin{bmatrix}i_d^*(k)\\ i_q^*(k)\end{bmatrix} \tag{9}$$

where $\mathbf{J}$ is the Jacobi matrix, which can be represented as

$$\mathbf{J}(k)=\begin{bmatrix}\frac{\partial f_1\left(i_d^*(k),i_q^*(k)\right)}{\partial i_d^*} & \frac{\partial f_1\left(i_d^*(k),i_q^*(k)\right)}{\partial i_q^*}\\ \frac{\partial f_2\left(i_d^*(k),i_q^*(k)\right)}{\partial i_d^*} & \frac{\partial f_2\left(i_d^*(k),i_q^*(k)\right)}{\partial i_q^*}\end{bmatrix}. \tag{10}$$

The convergence condition is

$$\left(i_d^*\left(k+1\right)-i_d^*(k)\right)^2+\left(i_q^*\left(k+1\right)-i_q^*(k)\right)^2<\varepsilon \tag{11}$$

where ε is iterative accuracy.

III. Proposed Improved Full-Speed Domain Control Method

A. Proposed MTPA and MTPV Criteria

The following mathematical expression can describe the MTPA optimal problem:

$$\min_{i_d,i_q} f=i_d^2+i_q^2$$

$$\text{s.t.}\begin{cases}T_e-\frac{3}{2}P_n\left(\psi_d i_q-\psi_d i_d\right)=0\\ i_d^2+i_q^2<I_{\lim}^2.\end{cases} \tag{12}$$

The MTPA problem (12) can be solved by the method of Lagrange multipliers, and the constructed Lagrange function is expressed as

$$F_{\text{MTPA}}\left(i_d,i_q,\lambda\right)=i_d^2+i_q^2+\lambda\left(\frac{3}{2}P_n\left(\psi_d\cdot i_q-\psi_q\cdot i_d\right)-T_{\text{ref}}\right). \tag{13}$$

Equating the partial derivatives of F_{MTPA} with respect to i_d, i_q, and λ to zero

$$\begin{aligned}\frac{\partial F_{\text{MTPA}}}{\partial i_d}&=2i_d+\lambda\frac{3}{2}P_n\left(\frac{\partial\psi_d}{\partial i_d}i_q-\frac{\partial\psi_q}{\partial i_d}i_d-\psi_q\right)=0\\ \frac{\partial F_{\text{MTPA}}}{\partial i_q}&=2i_q+\lambda\frac{3}{2}P_n\left(\frac{\partial\psi_d}{\partial i_q}i_q+\psi_d-\frac{\partial\psi_q}{\partial i_q}i_d\right)=0\\ \frac{\partial F_{\text{MTPA}}}{\partial\lambda}&=\frac{3}{2}P_n\left(\psi_d\cdot i_q-\psi_q\cdot i_d\right)-T_{\text{ref}}=0.\end{aligned} \tag{14}$$

The MTPA criterion proposed in this article considers the variation of inductances with current and the partial derivatives of the inductance with respect to current, as follows:

$$\psi_d i_d+\psi_q i_q+\left(\frac{\partial\psi_d}{\partial i_q}+\frac{\partial\psi_q}{\partial i_d}\right)i_d i_q-\frac{\partial\psi_q}{\partial i_q}i_d^2-\frac{\partial\psi_d}{\partial i_d}i_q^2=0. \tag{15}$$

The MTPV condition is to minimize the stator magnetic flux while achieving a reference torque. The MTPV optimal problem can be described as follows:

$$\min_{i_d,i_q} f=\psi_d^2+\psi_q^2$$

$$\text{s.t.}\begin{cases}T_e-\frac{3}{2}P_n\left(\psi_d i_q-\psi_q i_d\right)=0\\ \omega_e^2\left(\psi_d^2+\psi_q^2\right)<U_{\lim}^2.\end{cases} \tag{16}$$

The constructed Lagrange function is

$$F_{\text{MTPV}}\left(i_d,i_q,\lambda\right)=\psi_d^2+\psi_q^2+\lambda\left(\frac{3}{2}P_n\left(\psi_d\cdot i_q-\psi_q\cdot i_d\right)-T_{\text{ref}}\right). \tag{17}$$

The MTPV criterion proposed in this article is shown

$$\left(\psi_d i_d+\psi_q i_q\right)\left(\frac{\partial\psi_d}{\partial i_d}\frac{\partial\psi_q}{\partial i_q}-\frac{\partial\psi_d}{\partial i_q}\frac{\partial\psi_q}{\partial i_d}\right)-\psi_d^2\frac{\partial\psi_d}{\partial i_d}-\psi_q^2\frac{\partial\psi_q}{\partial i_q}-\psi_d\psi_q\left(\frac{\partial\psi_d}{\partial i_q}+\frac{\partial\psi_q}{\partial i_d}\right)=0. \tag{18}$$

Compared to the criterion of insufficient consideration of magnetic saturation in (5) and (7), the proposed criteria are essentially not neglected for the partial derivatives of the inductance with respect to current, i.e., $\frac{\partial L_d(i_d,i_q)}{\partial i_d}$, $\frac{\partial L_d(i_d,i_q)}{\partial i_q}$, $\frac{\partial L_q(i_d,i_q)}{\partial i_d}$, and $\frac{\partial L_q(i_d,i_q)}{\partial i_q}$. Fig. 2 gives the curves of MTPA and MTPV criteria, where model A corresponds to (4), (6), and

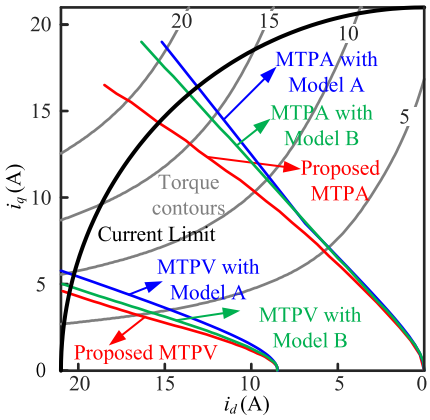

Fig. 2. MTPA and MTPV criteria of proposed and conventional methods.

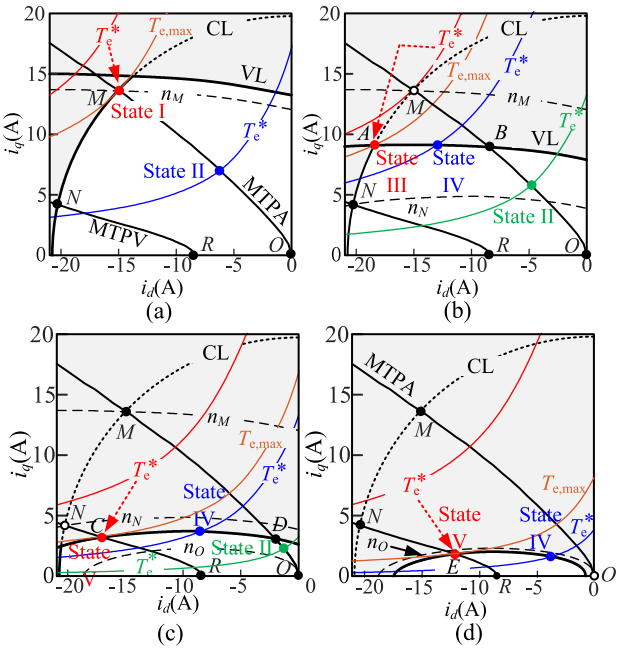

Fig. 3. Determination of the operation state for different T_e^*. (a) Branch I. (b) Branch II. (c) Branch III. (d) Branch IV.

model B corresponds to (5), (7). It follows that the proposed criterion has a significant deviation from the two conventional methods, which shows that neglecting the partial derivatives of the inductance with respect to current leads to a shift in the trajectory curves.

B. Flow Sequence

The flow sequence determines the operation branch and state based on the speed and reference torque, which has been described in detail in [9], [11], and [12]. The CL and VL are described, respectively, as

$$\begin{aligned} \sqrt{i_d^2+i_q^2} &\le I_{\lim} \\ \sqrt{(R_s i_d-\omega_e\psi_q)^2+(R_s i_q+\omega_e\psi_d)^2} &\le \tfrac{U_{dc}}{\sqrt{3}} \end{aligned} \tag{19}$$

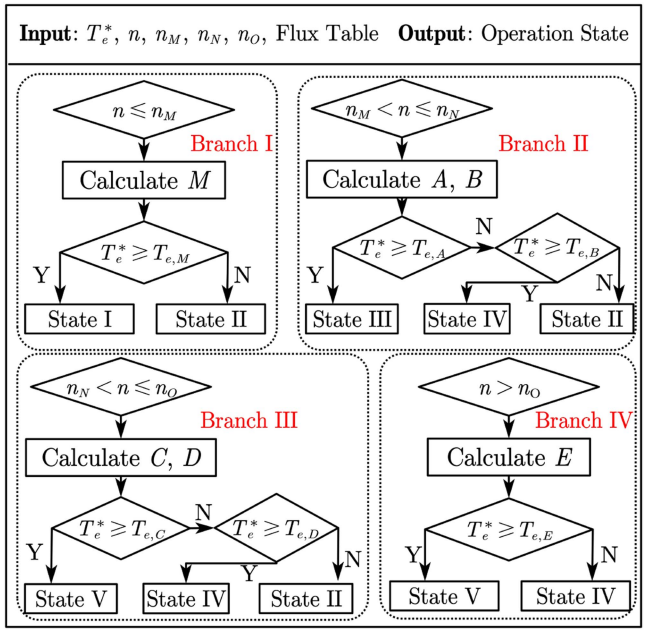

Fig. 4. Diagram of flow sequence.

where $I_{\lim}$ is CL value, U_{dc} is dc bus voltage. Fig. 3 gives the determination of the operation state for different reference torque T_e^* in different branches.

The block diagram of the flow sequence is given in Fig. 4. The online computational process requires solving the intersection equations for the operation point (OP) and the state demarcation points (SDPs), including M, A, B, C, D, and E. Among them, A, B, C, D, and E do not refer to specific points but to a class of points; for example, A represents the intersection of the VL curve with the left-side CL curve in Branch II.

The target functions and corresponding Jacobi matrices for the five states and six SDPs are shown in the Appendix, totalling six intersection cases. Compared to [9] and [11], the proposed method significantly increases the computational burden due to the more frequent use for lookup tables (LUTs). The bilinear interpolation algorithm can reduce the computational burden of each LUT, but its impact is still insignificant [9].

C. Proposed IIPOT

The N–R iterative method has local convergence and a local quadratic convergence rate. Within a particular range, initial iteration points that are closer relative to the convergence point tend to have fewer iteration times and higher convergence stability [26]. The iteration times plane for six intersection cases, given in Fig. 5, demonstrates this relationship.

1) IIPOT for SDPs: Based on Fig. 3, except M, SDPs represent the intersections of the VL curve with the curves on both sides, including CL, MTPA, and MTPV curves. SDPs are directly related to the motor operation speed and must be calculated in real time. The VL curve is affected mainly by motor speed, so it has a significant inertia characteristic, i.e., it hardly changes significantly during two consecutive computational periods (125 μs for 8 kHz). Fig. 6(a) and (b) gives the intersection

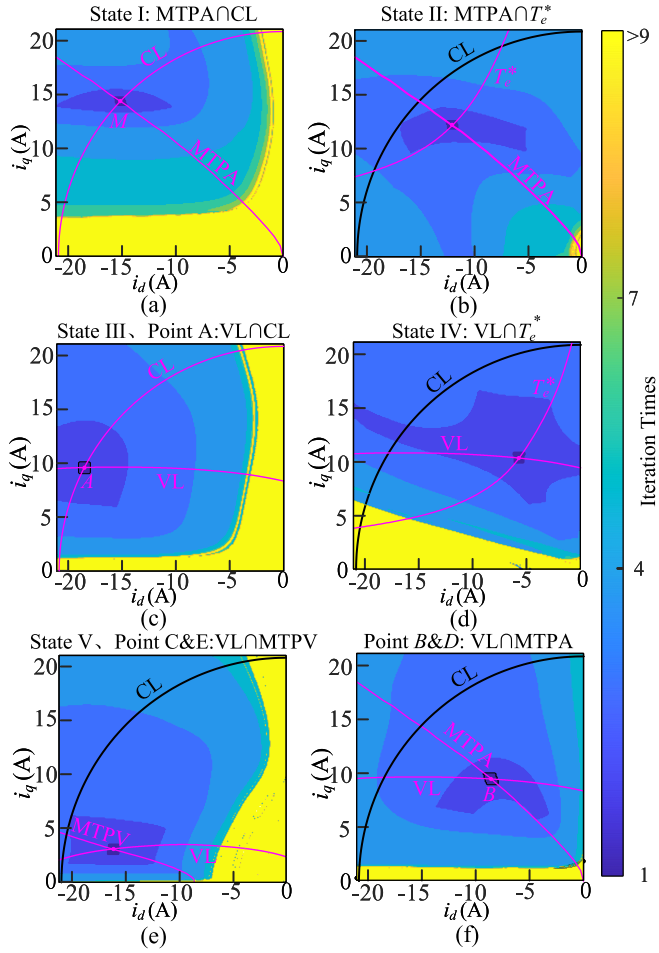

Fig. 5. Iteration times plane for different initial iteration points. (a) MTPA ∩ CL. (b) MTPA ∩ T_e^*. (c) VL ∩ CL. (d) VL ∩ T_e^*. (e) VL ∩ MTPV. (f) VL ∩ MTPA.

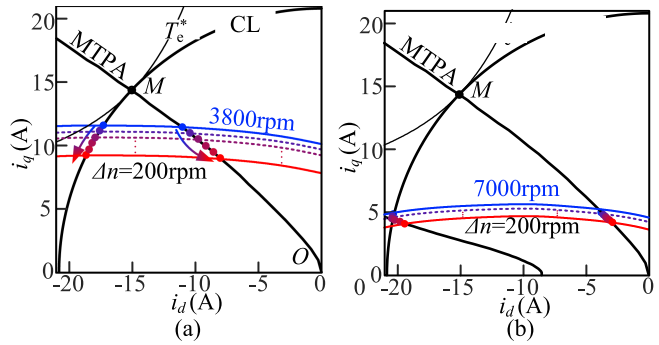

Fig. 6. Variation of SDPs in successive computation periods. (a) Δn = 200 r/min at 3800 r/min. (b) Δn = 200 r/min at 7000 r/min. (c) ΔU = 20 V at 3800 r/min. (d) ΔU = 20 V at 7000 r/min.

point change for Δn = 200 r/min at a speed of 3800 r/min and 7000 r/min, respectively. It can be seen that the SDPs are slowly moving during the successive calculations. Therefore, choosing the convergence result of the $(m-1)$th calculation period as the initial point of the mth calculation, as

$$i_{dq,x}^{\text{init}}(m) = i_{dq,x}^{*}(m-1) \tag{20}$$

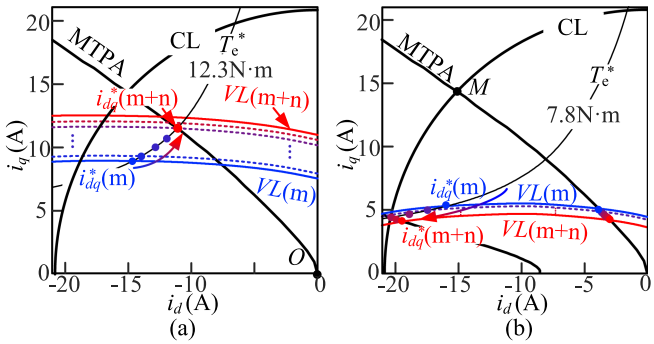

Fig. 7. Variation of OP in successive periods when T_e^* is unchanged. (a) Speed drop at T_e^* = 12.3 N · m. (b) Speed increase at T_e^* = 7.8 N · m.

where m denotes the mth computational period, $i_{dq,x}^{\text{init}}(m)$ is the initial iteration point of the mth computational period, and $i_{dq,x}^{*}(m-1)$ is the convergence point of the $(m-1)$th computational period. ($x = A, B, C, D, E$).

2) IIPOT for OP: During two consecutive computation periods, the change of OP depends on the change of reference torque. When the reference torque does not change in two consecutive calculations, the OP does not change significantly, even if the speed changes, as shown in Fig. 7(a) and (b). Considering the noise disturbances, set the torque threshold $T_{e,\text{th}}$ to 5% of rated torque. In this case, the convergence result of the last calculation period is chosen as the initial iteration point, as shown in (20). When the change in reference torque exceeds the threshold, a computational method is proposed based on the reference torque and the operation state, as follows.

When the operation states are I, III, and V, the OPs are M, A, and C, respectively. As shown in Fig. 3, they have been calculated during the SDPs computation, so recalculation is unnecessary.

When the operation state is IV, the OP is the intersection of the constant torque and the VL curves. According to Fig. 3, i_q varies less on the VL curve ($\overset{\frown}{AB}$, $\overset{\frown}{CD}$, $\overset{\frown}{EF}$), so torque variation ΔT_{e1} at the VL curve can be approximated as

$$\Delta T_{e1} \approx \frac{3}{2} P_n \left(L_d - L_q\right) i_q \cdot \Delta i_d \tag{21}$$

where Δi_d is d-axis current variation. The initial iteration point of the operating point Q can be designed based on the reference torque T_e^* and the SDPs, as follows:

$$\begin{aligned} i_{d,Q}^{\text{init}} &= \frac{T_e^* - T_{e,y}}{T_{e,x} - T_{e,y}} \left(i_{d,x} - i_{d,y}\right) + i_{d,y} \\ i_{q,Q}^{\text{init}} &= \frac{T_e^* - T_{e,y}}{T_{e,x} - T_{e,y}} \left(i_{q,x} - i_{q,y}\right) + i_{q,y} \end{aligned} \tag{22}$$

where y denotes the SDPs on the right side of the VL curve (B, D, F), and x denotes the SDPs on the left side (A, C, E). F is the intersection of the VL curve with the d-axis and is not included in the SDPs, but it can be calculated in the same way as the SDPs are calculated. As shown in Fig. 8, the proposed method approximates the curves $\overset{\frown}{AB}$, $\overset{\frown}{CD}$, and $\overset{\frown}{EF}$ as horizontal straight lines. The intersections of the straight lines $\overline{AB}$, $\overline{CD}$, and $\overline{EF}$

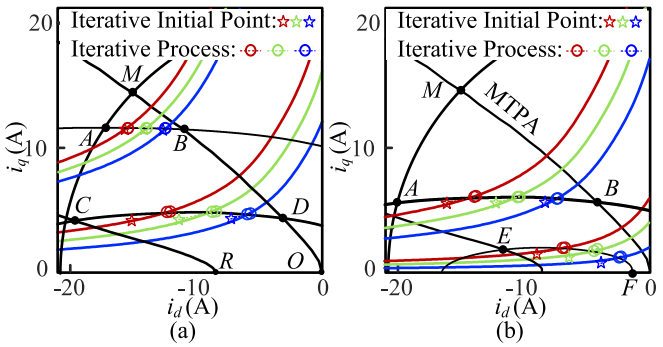

Fig. 8. Convergence process of proposed method in state IV when $T_e^* > T_{e,\text{th}}$. (a) AB and CD Curves. (b) AB and EF Curves.

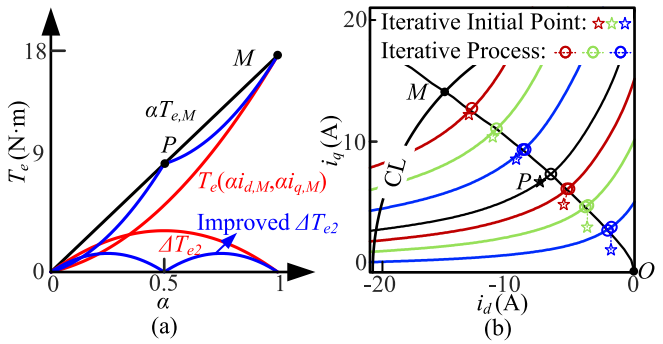

Fig. 9. Iterative analysis of proposed method in state II when $T_e^* > T_{e,\text{th}}$. (a) Analysis of torque errors. (b) Convergence process.

with the constant torque curve are used as the initial point. The iterative process of the proposed method is shown in Fig. 8.

When the operation state is II, the OP is the intersection of the constant torque and MTPA curves. Replacing the curve $\widehat{OM}$ with the straight line $\overline{OM}$, for the point $(\alpha \cdot i_{d,M}, \alpha \cdot i_{q,M})$ on the $\overline{OM}$, the difference between the calculated torque and $\alpha \cdot T_{e,M}$ is

$$\Delta T_{e2} = \left(\alpha - \alpha^2\right) \cdot \frac{3}{2} P_n \left(L_d - L_q\right) i_{d,M} i_{q,M}. \tag{23}$$

The ΔT_{e2} is maximum when α equals 0.5, indicating that under this condition, there is a maximum distance between the initial and convergence points. Unlike the ΔT_{e1}, ΔT_{e2} along the $\widehat{OM}$ has both d-axis and q-axis current variations. Therefore, an additional point P ($\alpha = 0.5$) is added, as shown in Fig. 9(a). Depending on the relationship between T_e^* and $T_{e,P}$, the linear interpolation method as described by (22) is used to obtain the initial points in the $\widehat{OP}$ and $\widehat{MP}$, respectively. The convergence process is given in Fig. 9(b).

IV. Experimental Results

Table I lists the parameters of the experimental PMaSynRM. Besides, Fig. 10 provides the dq-axis flux maps of experimental PMaSynRM, measured by the experimental method [21]. The nonlinear identification model of the inverter is based on [27], and the compensation method adopts the LUT method. The proposed control method is implemented digitally on the

TABLE I
PMaSynRM Parameters

Rated current	14.7 A
Rated speed	3000 r/min
Pole pairs	3
Phase resistance	0.41Ω
Permanent magnetic flux linkage	0.0629 V·s
Nominal d-axis inductance	7.4 mH
Nominal q-axis inductance	24.8 mH

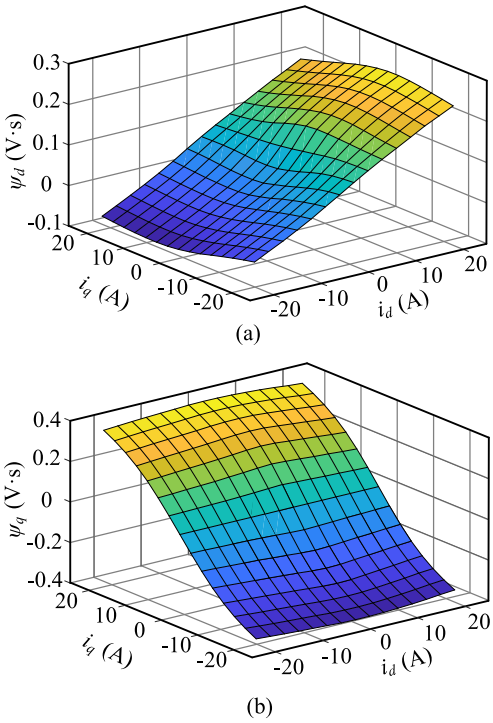

Fig. 10. dq-axis flux maps for the PMaSynRM. (a) d-axis. (b) q-axis.

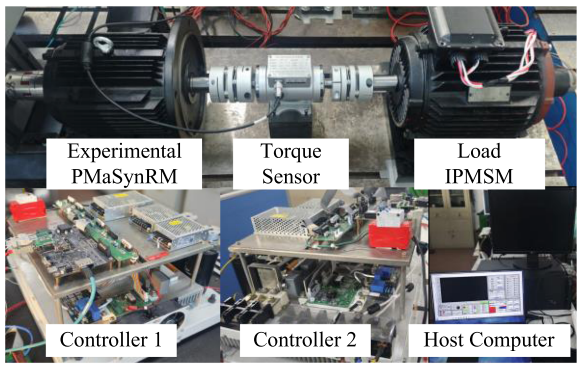

Fig. 11. Photographs of the experimental setup.

XMC4800, and the proposed full-speed domain control algorithm is synchronized with the system, operating at a control frequency of 8 kHz. The limit of iteration times is set to 4, and the iteration accuracy is 0.04. The experimental PMaSynRM is operated in torque-loop mode, and the load motor is operated in speed-loop mode. The photographs of the experimental setup are shown in Fig. 11, and the schematic diagram of the test bench is shown in Fig. 12.

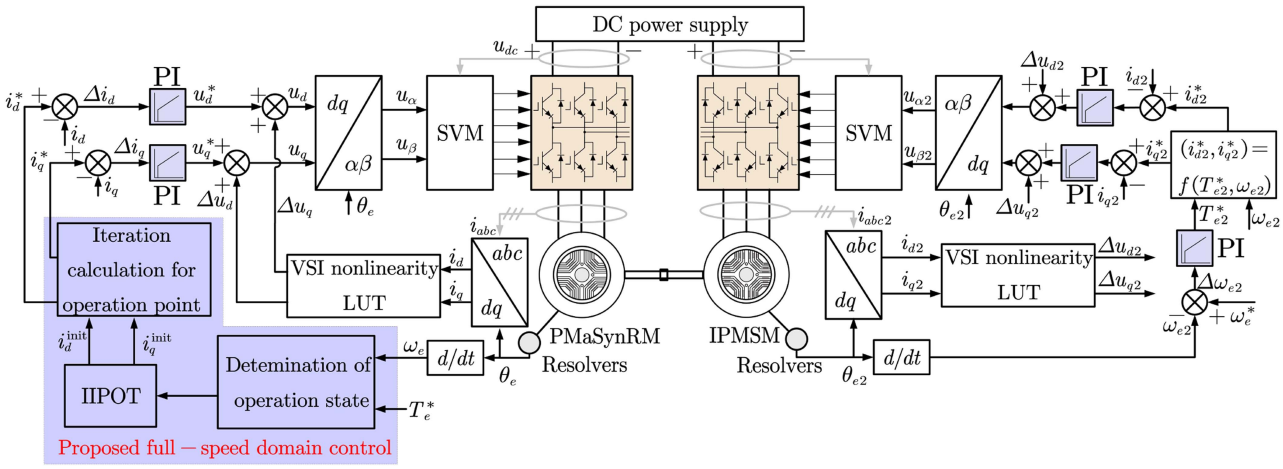

Fig. 12. Schematic diagram of the test bench.

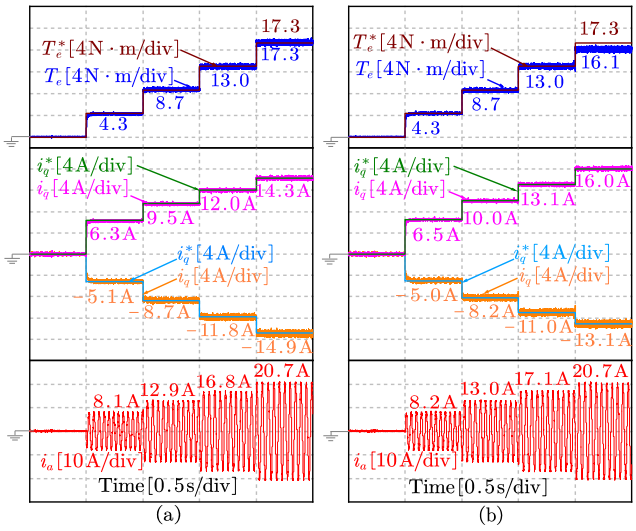

Fig. 13. Experimental waveforms of MTPA region. (a) Proposed MTPA criterion. (b) Compared MTPA criterion in [9] and [11].

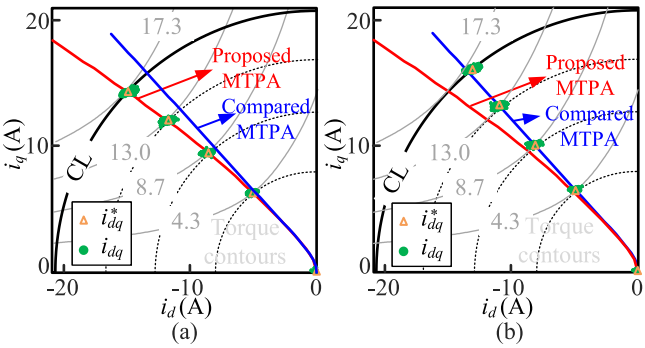

Fig. 14. Mapping for OPs in the current plane. (a) Proposed MTPA criterion. (b) Compared MTPA criterion in [9] and [11].

A. Verification and Comparison in MTPA Region

Figs. 13 and 14 show the experiment results for the MTPA region (State II), where (a) corresponds to the proposed MTPA criterion, and (b) corresponds to the MTPA criterion that ignores the partial derivative of the inductance with respect to current, as discussed in [9] and [11]. The operating speed is 500 r/min held by the load motor, while the reference torque is initially 0 and increases in steps until it reaches the maximum torque (17.3 N · m), which is measured a priori. According to Fig. 13(a), the reference dq-axis currents can rapidly respond to changes in the reference torque, and the actual currents can track the reference currents well. The experimental results are mapped to the current plane, as shown in Fig. 14(a), where the constant torque curves are obtained by a search method. The tangent points of the current circles and constant torque curves are located on the proposed MTPA trajectory, which indicates that the proposed criterion has the highest current utilization. Besides, the reference current points calculated by the proposed method are located on the proposed MTPA trajectory, which verifies the accuracy of the iterative calculation.

The same experimental conditions are set in the comparison test. According to Fig. 13(a) and (b), in the low torque region, the proposed criterion and the compared method have approximate current amplitude at the same torque output. As the load increases, the proposed method has a smaller current amplitude at the same torque output. When the current reaches the CL (20.7 A), the proposed method outputs a maximum torque of 17.3 N · m, while the comparison method outputs 16.1 N · m. The proposed method has a torque improvement of 7.4%.

B. Verification and Comparison in MTPV Region

Figs. 15 and 16 show the experiment results for the MTPV region (state V), where (a) corresponds to the proposed MTPV criterion, and (b) corresponds to the MTPV criterion that ignores partial derivatives of the inductance with respect to current, as discussed in [9] and [11]. The speed initially is 7000 r/min and increases linearly to 8000 r/min; the reference torque is set to 10 N· m. According to Fig. 15(a), the dq-axis current set-point initially is (−20.2 A, 5.0 A). As the speed rises, the dq-axis current point slides along the CL curve until it reaches the critical speed of the MTPV (7600 r/min), and the operation state is switched (III to V). Thereafter, as the speed rises, the d-axis begins to rise, and the q-axis current continues to decrease. The OP slides along the MTPV trajectory until the speed reaches a

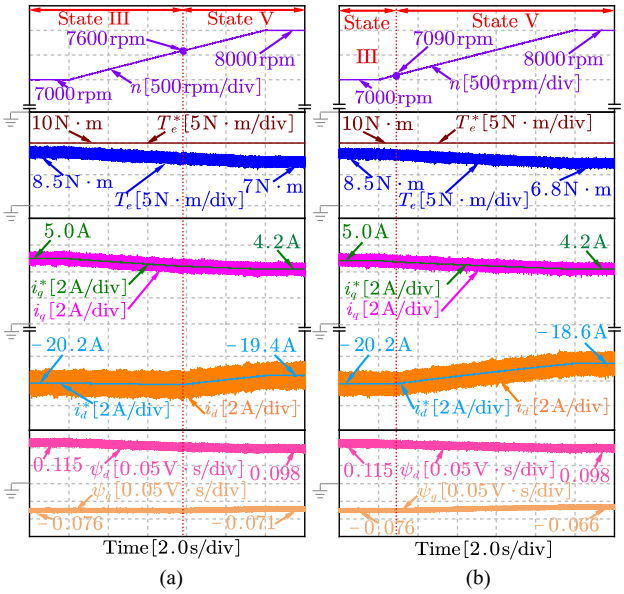

Fig. 15. Experimental waveforms of MTPV region. (a) Proposed MTPV criterion. (b) Compared MTPV criterion in [9] and [11].

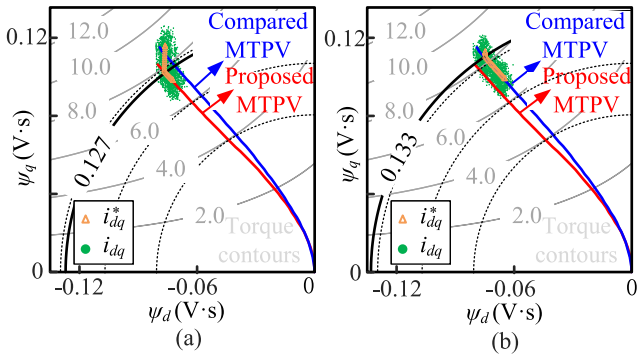

Fig. 16. Mapping for OPs in the magnetic flux plane. (a) Proposed MTPV criterion. (b) Compared MTPV criterion in [9] and [11].

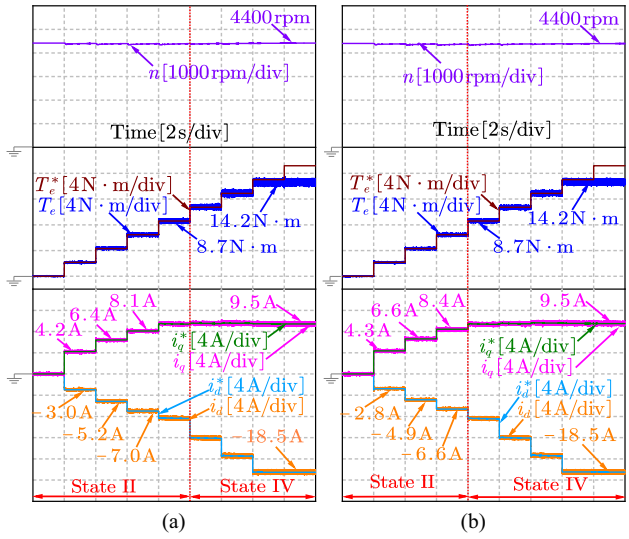

Fig. 17. Experimental results for switching process from state II to state IV. (a) Proposed method. (b) Compared method.

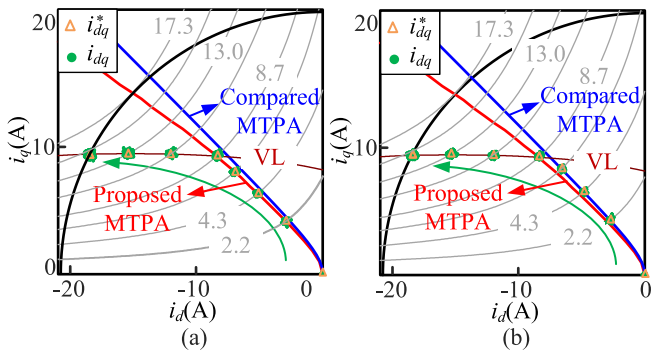

Fig. 18. Mapping results for the OP trajectory from state II to state IV. (a) Proposed method. (b) Compared method.

steady state (8000 r/min), at which time the dq-axis current point stabilizes at $(-19.4\ \text{A}, 4.2\ \text{A})$. Fig. 16(a) shows the experimental results mapped to the magnetic flux plane. The tangent points of the magnetic flux circles and constant torque curves are located on the proposed MTPV trajectory, which indicates that the proposed criterion has the highest flux utilization. Besides, the reference flux points are calculated by LUT and located on the proposed MTPV trajectory, verifying the accuracy of the iterative calculation.

In the comparison test, the same experimental conditions are set. According to Fig. 15(a) and (b), the MTPV speed threshold of the proposed method is 7600 r/min compared to 7090 r/min of the comparative method, which is 7.2% higher. Meanwhile, the proposed method has higher torque output under steady-state MTPV operation (e.g.: 7 N · m compared to 6.8 N · m at 8000 r/min).

C. Verification and Comparison of Remaining Regions

The effectiveness of the MTPA and the MTPV regions are verified in Parts A and B, respectively. In this part, the remaining states (states II, III, IV) and switching processes are verified as follows: 1) Increase the load torque at a constant speed (state II–state IV); 2) increase the speed gradually at a constant torque (state II-state IV-state III-state V).

Figs. 17 and 18 show the experiment and mapping results for the switching process from states II to IV, where (a) corresponds to the proposed method and (b) corresponds to the compared method discussed in [9] and [11]. The operating speed is 4400 r/min held by IPMSM, while the reference torque T_e^* is varied from 0 to 17.3 N · m in 8 steps. Fig. 18(a) and (b) presents the results mapped onto the current plane. For the proposed method shown in Fig. 18(a), during the first 10 s, the operation state is state II, and the OP steps along the MTPA trajectory as the reference torque increases. After 10 s, the VL limits the increase of the OP along the MTPA direction, and the OP then moves along the VL curve with a small change in the q-axis current and a significant decrease in the d-axis current. When the reference torque reaches 15.1 N· m, the OP moves to the intersection of the CL and VL curves, and the OP no longer changes.

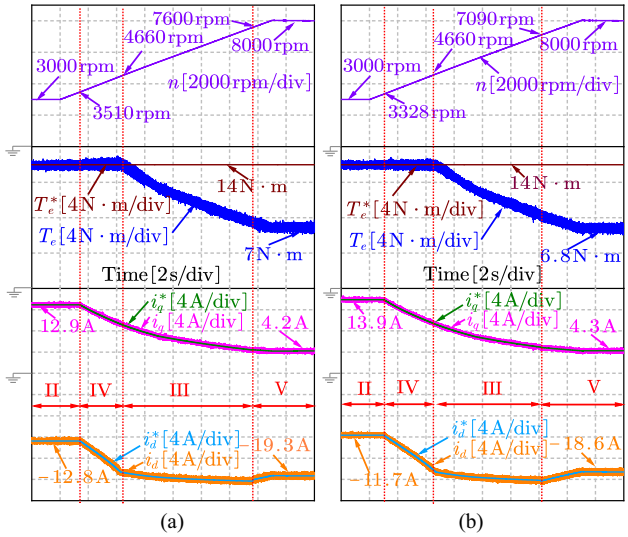

Fig. 19. Experimental results for operation process of state II-state IV-state III-state V. (a) Proposed method. (b) Compared method.

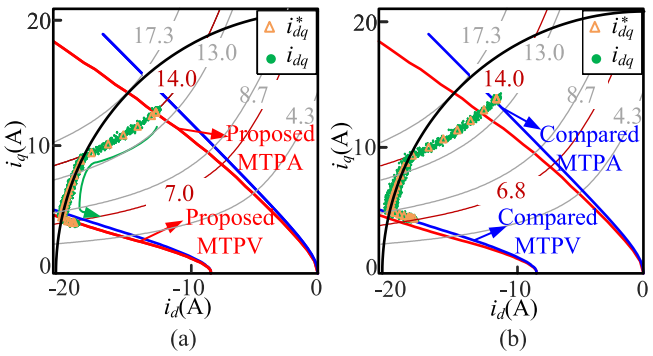

Fig. 20. Mapping results for the OP trajectory of state II-state IV-state III-state V. (a) Proposed method. (b) Compared method.

Fig. 18(a) and (b) demonstrates that both methods guarantee stable operation. When the reference torque T_e^* is greater than 8.7 N · m, the compared method has the same OP as the proposed method, as both methods have the same VL curve. Before 8.7 N · m, due to the differences in the MTPA trajectory between the two methods, the proposed method has a higher torque per ampere, resulting in lower copper losses.

Figs. 19 and 20 show the experiment results for the state II-state IV-state III-state V, where (a) corresponds to the proposed method, and (b) corresponds to the compared method discussed in [9], [11]. The operating speed, controlled by the IPMSM, is initially 3000 r/min and increases linearly to 8000 r/min. The reference torque T_e^* for experimental PMaSynRM is set to 14 N · m. Fig. 20(a) presents the results mapped onto the current plane. Before 3.8 s, the VL has not yet constrained the OP. The dq-axis currents are constant at −12.8 A and 12.9 A, respectively, and the operation state is state II. As the speed increases, the OP slides along the 14 N · m constant torque curve, and the amplitude of the d-axis current increases while the q-axis current decreases. The OP moves far from the MTPA curve until it reaches the CL curve. After that, the output torque fails to meet the reference torque. As the speed increases, the VL curve continues to downshift, the OP slides along the CL curve, and the output torque cannot track the reference torque, i.e., operation state III. Until the OP reaches the intersection of the MTPV and CL curve, the OP starts sliding along the MTPV curve, and the amplitude of the d-axis current transitions from increasing to slightly decreasing while the q-axis current continues to decrease, i.e., state V.

Figs. 19 and 20 demonstrate that both methods guarantee stable operation. The difference depends on the changes in the switching points due to the different MTPA and MTPV trajectories. According to Fig. 19(b), the comparative method switches from state II to state IV at a lower speed (3328 r/min compared to 3510 r/min). The comparison indicates that the proposed method has a wider speed range in the MTPA region, enabling it to achieve higher efficiency over a broader speed range (0 to 3510 r/min). In addition, the proposed method enters the MTPV operation region only after the speed reaches 7600 r/min, which is a 7.2% increase compared to the critical speed of 7090 r/min

TABLE II
COMPUTATIONAL TIME FOR DIFFERENT INTERSECTIONS IN A SINGLE ITERATION OF PROPOSED METHOD

Case	Time	Case	Time
MTPA ∩ CL	14.2 μs	MTPA ∩ T_e^*	14.8 μs
VL ∩ CL	14.6 μs	VL ∩ T_e^*	15.7 μs
VL ∩ MTPV	18.4 μs	VL ∩ MTPA	16.7 μs

TABLE III
COMPARISON OF THE PROPOSED METHOD BASED IIPOT AND THE PROPOSED METHOD EXCEPT IIPOT

Branch-State	Method based on IIPOT Iteration times/time		Method except IIPOT
	$\Delta T_e > T_{e,\text{th}}$	$\Delta T_e \leq T_{e,\text{th}}$	
I-I	0-0-0/8.7 μs	0-0-0/8.7 μs	0-0-0/8.7 μs
I-II	0-0-2/37.2 μs	0-0-1/25.4 μs	0-0-4/66.8 μs
II-III	1-1-0/51.6 μs	1-1-0/51.0 μs	3-3-0/112.2 μs
II-IV	1-1-1/69.5 μs	1-1-1/68.0 μs	3-3-4/176.2 μs
II-II	1-1-2/84.5 μs	1-1-1/68.5 μs	3-3-4/181.0 μs
III-V	1-1-0/57.5 μs	1-1-0/57.5 μs	3-3-0/127.1 μs
III-IV	1-1-2/89.5 μs	1-1-1/74.5 μs	3-3-4/190.5 μs
III-II	1-1-2/89.5 μs	1-1-1/74.0 μs	3-3-4/185.7 μs
IV-V	1-0-0/42.0 μs	1-0-0/42.0 μs	3-0-0/78.8 μs
IV-IV	1-1-2/88.5 μs	1-1-1/74.5 μs	3-3-4/180.6 μs

TABLE IV
ITERATION TIMES/TIME OF THE PROPOSED METHOD AND COMPARED METHOD IN [9] AND [11]

Branch-State	Proposed method Iteration times/time		Compared method Iteration times/time
	$\Delta T_e > T_{e,\text{th}}$	$\Delta T_e \leq T_{e,\text{th}}$	
I-I	0-0-0/8.7 μs	0-0-0/8.7 μs	0-0-0/8.7 μs
I-II	0-0-2/37.2 μs	0-0-1/25.4 μs	0-0-4/46.8 μs
II-III	1-1-0/51.6 μs	1-1-0/51.0 μs	3-3-0/88.7 μs
II-IV	1-1-1/69.5 μs	1-1-1/68.0 μs	3-3-4/136.5 μs
II-II	1-1-2/84.5 μs	1-1-1/68.5 μs	3-3-4/138.5 μs
III-V	1-1-0/57.5 μs	1-1-0/57.5 μs	3-3-0/101.0 μs
III-IV	1-1-2/89.5 μs	1-1-1/74.5 μs	3-3-4/147.2 μs
III-II	1-1-2/89.5 μs	1-1-1/74.0 μs	3-3-4/142.4 μs
IV-V	1-0-0/42.0 μs	1-0-0/42.0 μs	3-0-0/65.6 μs
IV-IV	1-1-2/88.5 μs	1-1-1/74.5 μs	3-0-4/112.3 μs

TABLE V
TARGET FUNCTIONS AND JACOBI MATRICES FOR DIFFERENT OPERATION STATES

State I : MTPA ∩ CL $\begin{cases} f_1\left(i_d^*, i_q^*\right) = \left(\psi_d i_d^* + \psi_q i_q^*\right) - \frac{\partial \psi_q}{\partial i_q} i_d^{*2} \\ + \left(\frac{\partial \psi_d}{\partial i_q} + \frac{\partial \psi_q}{\partial i_d}\right) i_d^* i_q^* - \frac{\partial \psi_d}{\partial i_d} i_q^{*2} = 0 \\ f_2\left(i_d^*, i_q^*\right) = i_d^{*2} + i_q^{*2} - I_{\lim}^2 = 0 \end{cases}$	$\begin{bmatrix} \left(\frac{\partial \psi_d}{\partial i_q} + \frac{\partial \psi_q}{\partial i_d}\right) i_q - 2\frac{\partial \psi_q}{\partial i_q} i_d & \left(\frac{\partial \psi_d}{\partial i_q} + \frac{\partial \psi_q}{\partial i_d}\right) i_d - 2\frac{\partial \psi_d}{\partial i_d} i_q \\ + \frac{\partial \psi_d}{\partial i_d} i_d + \psi_d + \frac{\partial \psi_q}{\partial i_d} i_q & + \frac{\partial \psi_d}{\partial i_q} i_d + \psi_q + \frac{\partial \psi_q}{\partial i_q} i_q \\ \hline 2i_d & 2i_q \end{bmatrix}$
State II : MTPA ∩ T_e^* $\begin{cases} f_1\left(i_d^*, i_q^*\right) = \left(\psi_d i_d^* + \psi_q i_q^*\right) - \frac{\partial \psi_q}{\partial i_q} i_d^{*2} \\ + \left(\frac{\partial \psi_d}{\partial i_q} + \frac{\partial \psi_q}{\partial i_d}\right) i_d^* i_q^* - \frac{\partial \psi_d}{\partial i_d} i_q^{*2} = 0 \\ f_2\left(i_d^*, i_q^*\right) = \frac{3}{2} P_n \left(\psi_d i_q^* - \psi_q i_d^*\right) - T_e^* = 0 \end{cases}$	$\begin{bmatrix} \left(\frac{\partial \psi_d}{\partial i_q} + \frac{\partial \psi_q}{\partial i_d}\right) i_q - 2\frac{\partial \psi_q}{\partial i_q} i_d & \left(\frac{\partial \psi_d}{\partial i_q} + \frac{\partial \psi_q}{\partial i_d}\right) i_d - 2\frac{\partial \psi_d}{\partial i_d} i_q \\ + \frac{\partial \psi_d}{\partial i_d} i_d + \psi_d + \frac{\partial \psi_q}{\partial i_d} i_q & + \frac{\partial \psi_d}{\partial i_q} i_d + \psi_q + \frac{\partial \psi_q}{\partial i_q} i_q \\ \frac{3}{2} P_n \left(\frac{\partial \psi_d}{\partial i_d} i_q - \frac{\partial \psi_q}{\partial i_d} i_d - \psi_q\right) & \frac{3}{2} P_n \left(\frac{\partial \psi_d}{\partial i_q} i_q - \frac{\partial \psi_q}{\partial i_q} i_d + \psi_d\right) \end{bmatrix}$
State III, Point A : VL ∩ CL $\begin{cases} f_1\left(i_d^*, i_q^*\right) = \left(R_s i_d - \omega_e \psi_q\right)^2 \\ + \left(R_s i_q + \omega_e \psi_d\right)^2 - \left(\frac{U_{dc}}{\sqrt{3}}\right)^2 = 0 \\ f_2\left(i_d^*, i_q^*\right) = i_d^{*2} + i_q^{*2} - I_{\lim}^2 = 0 \end{cases}$	$\begin{bmatrix} 2\left(R_s i_d - \omega_e \psi_q\right)\left(R_s - \omega_e \frac{\partial \psi_q}{\partial i_d}\right) & 2\left(R_s i_q + \omega_e \psi_d\right)\left(R_s + \omega_e \frac{\partial \psi_d}{\partial i_q}\right) \\ + 2\omega_e \left(R_s i_q + \omega_e \psi_d\right) \frac{\partial \psi_d}{\partial i_d} & - 2\omega_e \left(R_s i_d - \omega_e \psi_q\right) \frac{\partial \psi_q}{\partial i_q} \\ \hline 2i_d & 2i_q \end{bmatrix}$
State IV : VL ∩ T_e^* $\begin{cases} f_1\left(i_d^*, i_q^*\right) = \left(R_s i_d - \omega_e \psi_q\right)^2 \\ + \left(R_s i_q + \omega_e \psi_d\right)^2 - \left(\frac{U_{dc}}{\sqrt{3}}\right)^2 = 0 \\ f_2\left(i_d^*, i_q^*\right) = \frac{3}{2} P_n \left(\psi_d i_q - \psi_q i_d\right) - T_e^* = 0 \end{cases}$	$\begin{bmatrix} 2\left(R_s i_d - \omega_e \psi_q\right)\left(R_s - \omega_e \frac{\partial \psi_q}{\partial i_d}\right) & 2\left(R_s i_q + \omega_e \psi_d\right)\left(R_s + \omega_e \frac{\partial \psi_d}{\partial i_q}\right) \\ + 2\omega_e \left(R_s i_q + \omega_e \psi_d\right) \frac{\partial \psi_d}{\partial i_d} & - 2\omega_e \left(R_s i_d - \omega_e \psi_q\right) \frac{\partial \psi_q}{\partial i_q} \\ \frac{3}{2} P_n \left(\frac{\partial \psi_d}{\partial i_d} i_q - \frac{\partial \psi_q}{\partial i_d} i_d - \psi_q\right) & \frac{3}{2} P_n \left(\frac{\partial \psi_d}{\partial i_q} i_q - \frac{\partial \psi_q}{\partial i_q} i_d + \psi_d\right) \end{bmatrix}$
State V, Point C, E : VL ∩ MTPV $\begin{cases} f_1\left(i_d^*, i_q^*\right) = \left(R_s i_d - \omega_e \psi_q\right)^2 \\ + \left(R_s i_q + \omega_e \psi_d\right)^2 - \left(\frac{U_{dc}}{\sqrt{3}}\right)^2 = 0 \\ f_2\left(i_d^*, i_q^*\right) = -\psi_d^2 \frac{\partial \psi_d}{\partial i_d} - \psi_q^2 \frac{\partial \psi_q}{\partial i_q} \\ + \left(\psi_d i_d + \psi_q i_q\right)\left(\frac{\partial \psi_d}{\partial i_d} \frac{\partial \psi_q}{\partial i_q} - \frac{\partial \psi_d}{\partial i_q} \frac{\partial \psi_q}{\partial i_d}\right) \\ - \psi_d \psi_q \frac{\partial \psi_d}{\partial i_q} \frac{\partial \psi_q}{\partial i_d} = 0 \end{cases}$	$\begin{bmatrix} 2\left(R_s i_d - \omega_e \psi_q\right)\left(R_s - \omega_e \frac{\partial \psi_q}{\partial i_d}\right) & 2\left(R_s i_q + \omega_e \psi_d\right)\left(R_s + \omega_e \frac{\partial \psi_d}{\partial i_q}\right) \\ + 2\omega_e \left(R_s i_q + \omega_e \psi_d\right) \frac{\partial \psi_d}{\partial i_d} & - 2\omega_e \left(R_s i_d - \omega_e \psi_q\right) \frac{\partial \psi_q}{\partial i_q} \\ \left(\frac{\partial \psi_d}{\partial i_d} i_d + \psi_d + \frac{\partial \psi_q}{\partial i_d} i_q\right)\left(\frac{\partial \psi_d}{\partial i_d} \frac{\partial \psi_q}{\partial i_q} - \frac{\partial \psi_d}{\partial i_q} \frac{\partial \psi_q}{\partial i_d}\right) & \left(\frac{\partial \psi_d}{\partial i_q} i_d + \psi_q + \frac{\partial \psi_q}{\partial i_q} i_q\right)\left(\frac{\partial \psi_d}{\partial i_d} \frac{\partial \psi_q}{\partial i_q} - \frac{\partial \psi_d}{\partial i_q} \frac{\partial \psi_q}{\partial i_d}\right) \\ - 2\psi_d \left(\frac{\partial \psi_d}{\partial i_d}\right)^2 - 2\psi_q \frac{\partial \psi_q}{\partial i_d} \frac{\partial \psi_q}{\partial i_q} & - 2\psi_d \frac{\partial \psi_d}{\partial i_q} \frac{\partial \psi_d}{\partial i_d} - 2\psi_q \left(\frac{\partial \psi_q}{\partial i_q}\right)^2 \\ - \left(\psi_q \frac{\partial \psi_d}{\partial i_d} + \psi_d \frac{\partial \psi_q}{\partial i_d}\right)\left(\frac{\partial \psi_d}{\partial i_q} + \frac{\partial \psi_q}{\partial i_d}\right) & - \left(\psi_q \frac{\partial \psi_d}{\partial i_q} + \psi_d \frac{\partial \psi_q}{\partial i_q}\right)\left(\frac{\partial \psi_d}{\partial i_q} + \frac{\partial \psi_q}{\partial i_d}\right) \end{bmatrix}$
Point B, D : VL ∩ MTPA $\begin{cases} f_1\left(i_d^*, i_q^*\right) = \left(R_s i_d - \omega_e \psi_q\right)^2 \\ + \left(R_s i_q + \omega_e \psi_d\right)^2 - \left(\frac{U_{dc}}{\sqrt{3}}\right)^2 = 0 \\ f_2\left(i_d^*, i_q^*\right) = \left(\psi_d i_d + \psi_q i_q\right) - \frac{\partial \psi_q}{\partial i_q} i_d^2 \\ + \left(\frac{\partial \psi_d}{\partial i_q} + \frac{\partial \psi_q}{\partial i_d}\right) i_d i_q - \frac{\partial \psi_d}{\partial i_d} i_q^2 = 0 \end{cases}$	$\begin{bmatrix} 2\left(R_s i_d - \omega_e \psi_q\right)\left(R_s - \omega_e \frac{\partial \psi_q}{\partial i_d}\right) & 2\left(R_s i_q + \omega_e \psi_d\right)\left(R_s + \omega_e \frac{\partial \psi_d}{\partial i_q}\right) \\ + 2\omega_e \left(R_s i_q + \omega_e \psi_d\right) \frac{\partial \psi_d}{\partial i_d} & - 2\omega_e \left(R_s i_d - \omega_e \psi_q\right) \frac{\partial \psi_q}{\partial i_q} \\ \left(\frac{\partial \psi_d}{\partial i_q} + \frac{\partial \psi_q}{\partial i_d}\right) i_q - 2\frac{\partial \psi_q}{\partial i_q} i_d & \left(\frac{\partial \psi_d}{\partial i_q} + \frac{\partial \psi_q}{\partial i_d}\right) i_d - 2\frac{\partial \psi_d}{\partial i_d} i_q \\ + \frac{\partial \psi_d}{\partial i_d} i_d + \psi_d + \frac{\partial \psi_q}{\partial i_d} i_q & + \frac{\partial \psi_d}{\partial i_q} i_d + \psi_q + \frac{\partial \psi_q}{\partial i_q} i_q \end{bmatrix}$

for the compared method. It indicates that the proposed method has a stronger capability for speed extension.

D. Verification and Comparison on Computation Burden

The total computation time for the proposed full-speed control algorithm includes four parts: branch judgment, SDPs computation, state judgment, and OP computation. Among these, the SDPs computation and the OP computation require multiple iterations, which occupy the main computation time. Table II provides the computational time for a single iteration of the six intersection cases.

The IIPOT utilized depends on whether T_e^* exceeds the thresholds, even if the OPs are in the same branch and operation state. In order to fully validate the effectiveness of the proposed IIPOT in all cases, experimental tests and comparisons are performed for all branch-states. Table III gives the iteration times [SDPs(left)—SDPs(right)—OP] and total online computation time obtained from the experimental test. The iteration times of 0 means that no iterative computation is executed. When $\Delta T_e < T_{e,\text{th}}$, only one iteration is required to converge. On the contrary, when $\Delta T_e > T_{e,\text{th}}$, the proposed method also converges in two iterations. The average computation time of the proposed method decreases by 68.7 μs compared to the method without IIPOT. The execution time of the proposed method satisfies the real-time requirements at 8 kHz (125 μs).

To fully illustrate the proposed method's superiority, the computational burden of the proposed method is compared with [9], [11] in all branch-states, as shown in Table IV. The comparison shows that the proposed method has superior computational efficiency in almost all cases.

V. CONCLUSION

In this article, a computationally efficient full-speed domain control method for PMaSynRM considering magnetic saturation is proposed. The novelty of this method lies in its adoption of a more accurate MTPA and MTPV criteria, which considers the partial derivative of inductance with respect to current, as well as an IIPOT, which reduces the computational burden of iterative calculations. The experimental results show that the proposed method has a maximum torque improvement of 7.4% in the MTPA operation region and increases the MTPV critical speed by 7.2% in the MTPV operation region while outputting a larger torque. The maximum computation time of the proposed algorithm is 89.5 μs, which ensures real-time computation in an 8 kHz control system.

APPENDIX

The target functions and Jacobi Matrices for different operation state is shown in Table V.

REFERENCES

[1] G. Xu, Z. Jia, Q. Chen, J. Xia, Y. Cai, and Z. Zhang, "A fast and effective optimization procedure for the ferrite PMaSynRM to reduce material cost," *IEEE Trans. Transport. Electrific.*, vol. 10, no. 1, pp. 635–647, Mar. 2024.

[2] M. Zhao, Z. Liu, Q. Chen, G. Liu, X. Zhu, and J. Zhang, "Fault-tolerant control of a triple redundant PMa-SynRM for minimum torque ripple," *IEEE Trans. Transport. Electrific.*, vol. 10, no. 1, pp. 999–1011, Mar. 2024.

[3] S. Kim, Y.-D. Yoon, S.-K. Sul, and K. Ide, "Maximum torque per ampere (MTPA) control of an IPM machine based on signal injection considering inductance saturation," *IEEE Trans. Power Electron.*, vol. 28, no. 1, pp. 488–497, Jan. 2013.
[4] J. Wang et al., "An accurate virtual signal injection control of MTPA for an IPMSM with fast dynamic response," *IEEE Trans. Power Electron.*, vol. 33, no. 9, pp. 7916–7926, Sep. 2018.
[5] A. Dianov and A. Anuchin, "Adaptive maximum torque per ampere control for IPMSM drives with load varying over mechanical revolution," *IEEE Trans. Emerg. Sel. Topics Power Electron.*, vol. 10, no. 3, pp. 3409–3417, Jun. 2022.
[6] G. Feng, C. Lai, Y. Han, and N. C. Kar, "Fast maximum torque per ampere (MTPA) angle detection for interior PMSMS using online polynomial curve fitting," *IEEE Trans. Power Electron.*, vol. 37, no. 2, pp. 2045–2056, Feb. 2022.
[7] S. Bozhko, M. Rashed, C. I. Hill, S. S. Yeoh, and T. Yang, "Flux-weakening control of electric starter–generator based on permanent-magnet machine," *IEEE Trans. Transport. Electrific.*, vol. 3, no. 4, pp. 864–877, Dec. 2017.
[8] M. Tursini, E. Chiricozzi, and R. Petrella, "Feedforward flux-weakening control of surface-mounted permanent-magnet synchronous motors accounting for resistive voltage drop," *IEEE Trans. Ind. Electron.*, vol. 57, no. 1, pp. 440–448, Jan. 2010.
[9] S. Wang, J. Kang, M. Degano, A. Galassini, and C. Gerada, "An accurate wide-speed range control method of IPMSM considering resistive voltage drop and magnetic saturation," *IEEE Trans. Ind. Electron.*, vol. 67, no. 4, pp. 2630–2641, Apr. 2020.
[10] J. Bonifacio and R. M. Kennel, "On considering saturation and cross-coupling effects for copper loss minimization on highly anisotropic synchronous machines," *IEEE Trans. Ind. Appl.*, vol. 54, no. 5, pp. 4177–4185, May 2018.
[11] Y. Lu, S. He, C. Li, H. Luo, H. Yang, and R. Zhao, "Online full-speed region control method of IPMSM drives considering cross-saturation inductances and stator resistance," *IEEE Trans. Transport. Electrific.*, vol. 9, no. 2, pp. 3164–3176, Jun. 2023.
[12] Z. Xia, S. Nalakath, R. Tarvirdilu-Asl, Y. Sun, J. Wiseman, and A. Emadi, "Online optimal tracking method for interior permanent magnet machines with improved MTPA and MTPV in whole speed and torque ranges," *IEEE Trans. Power Electron.*, vol. 35, no. 9, pp. 9753–9769, Sep. 2020.
[13] C. Miguel-Espinar, D. Heredero-Peris, R. Villafafila-Robles, and D. Montesinos-Miracle, "Review of flux-weakening algorithms to extend the speed range in electric vehicle applications with permanent magnet synchronous machines," *IEEE Access*, vol. 11, pp. 22961–22981, 2023.
[14] A. Consoli, G. Scelba, G. Scarcella, and M. Cacciato, "An effective energy-saving scalar control for industrial IPMSM drives," *IEEE Trans. Ind. Electron.*, vol. 60, no. 9, pp. 3658–3669, Sep. 2013.
[15] A. Accetta, M. Cirrincione, M. C. Di Piazza, G. La Tona, M. Luna, and M. Pucci, "Analytical formulation of a maximum torque per ampere (MTPA) technique for SynRMs considering the magnetic saturation," *IEEE Trans. Ind. Appl.*, vol. 56, no. 4, pp. 3846–3854, Jul./Aug. 2020.
[16] A. E. Hoffer, R. H. Moncada, B. J. Pavez-Lazo, J. A. Tapia, and L. Laurila, "Calculation of a current vector trajectory for enhanced operation of synchronous reluctance generators including saturation," *IEEE Trans. Ind. Electron.*, vol. 70, no. 2, pp. 1197–1204, Feb. 2023.
[17] A. Rabiei, T. Thiringer, M. Alatalo, and E. A. Grunditz, "Improved maximum-torque-per-ampere algorithm accounting for core saturation, cross-coupling effect, and temperature for a PMSM intended for vehicular applications," *IEEE Trans. Transport. Electrific.*, vol. 2, no. 2, pp. 150–159, Jun. 2016.
[18] T. A. Huynh and M.-F. Hsieh, "Comparative study of PM-assisted SynRM and IPMSM on constant power speed range for EV applications," *IEEE Trans. Magn.*, vol. 53, no. 11, Nov. 2017, Art. no. 8211006.
[19] P. Niazi, H. A. Toliyat, and A. Goodarzi, "Robust maximum torque per ampere (MTPA) control of pm-assisted SynRM for traction applications," *IEEE Trans. Veh. Technol.*, vol. 56, no. 4, pp. 1538–1545, Jul. 2007.
[20] C. Lai, G. Feng, K. Mukherjee, J. Tjong, and N. C. Kar, "Maximum torque per ampere control for IPMSM using gradient descent algorithm based on measured speed harmonics," *IEEE Trans. Ind. Inform.*, vol. 14, no. 4, pp. 1424–1435, Apr. 2018.
[21] E. Armando, R. I. Bojoi, P. Guglielmi, G. Pellegrino, and M. Pastorelli, "Experimental identification of the magnetic model of synchronous machines," *IEEE Trans. Ind. Appl.*, vol. 49, no. 5, pp. 2116–2125, Sep./Oct. 2013.
[22] Q. Liu and K. Hameyer, "High-performance adaptive torque control for an IPMSM with real-time MTPA operation," *IEEE Trans. Energy Convers.*, vol. 32, no. 2, pp. 571–581, Jun. 2017.
[23] Q. Xu and L. Cai, "Developing an approach in calculating reference currents for field-weakening control," *IEEE Trans. Transport. Electrific.*, vol. 9, no. 1, pp. 60–74, Mar. 2023.
[24] B. Cheng and T. R. Tesch, "Torque feedforward control technique for permanent-magnet synchronous motors," *IEEE Trans. Ind. Electron.*, vol. 57, no. 3, pp. 969–974, Mar. 2010.
[25] H. Liu, Z. Q. Zhu, E. Mohamed, Y. Fu, and X. Qi, "Flux-weakening control of nonsalient pole PMSM having large winding inductance, accounting for resistive voltage drop and inverter nonlinearities," *IEEE Trans. Power Electron.*, vol. 27, no. 2, pp. 942–952, Feb. 2012.
[26] S. Chen, W. Ding, R. Hu, X. Wu, and S. Shi, "Sensorless control of PMSM drives using reduced order quasi resonant-based ESO and Newton-Raphson method-based PLL," *IEEE Trans. Power Electron.*, vol. 38, no. 1, pp. 229–244, Jan. 2023.
[27] B. Zhong, J. Su, K. Tan, and G. Yang, "Offline identification of VSI nonlinearity at arbitrary initial angles based on inverter modeling," *IEEE Trans. Energy Convers.*, vol. 39, no. 2, pp. 1423–1435, Jun. 2024.

Kaiwen Tan received the B.E. degree in electrical engineering in 2019 from the Shenyang University of Technology, Shenyang, China, and the M.E. degree in electrical engineering in 2021 from the Harbin Institute of Technology, Harbin, China, where he is currently working toward the Ph.D. degree in electrical engineering.

His research interests include parameter identification and motor control for permanent magnet-assisted synchronous reluctance motor and synchronous reluctance motor.

Jianyong Su (Member, IEEE) was born in China, in 1979. He received the B.S., M.S., and Ph.D. degrees in electrical engineering from the Harbin Institute of Technology (HIT), Harbin, China, in 2002, 2004, and 2009, respectively.

He is currently an Associate Professor with the School of Electrical Engineering and Automation, HIT. From 2015 to 2016, he was a Visiting Scholar with the North Carolina State University, Raleigh, NC, USA. His research interests include permanent magnet synchronous motor (PMSM), multiphase PMSM, synchronous reluctance motor (SynRM), sensorless control, and field-weakening control.

Bencheng Zhong received the B.S. degree in electrical engineering in 2018 from the Harbin Institute of Technology (HIT), Harbin, China, where he is currently working toward the Ph.D. degree in electrical engineering.

His current research interests include electric machines and drives with emphasis on self-commissioning and optimal control for synchronous reluctance machines and switched reluctance machines.

Guijie Yang was born in China, in 1965. He received the Ph.D. degree in electrical engineering from the Harbin Institute of Technology (HIT), Harbin, China, in 2001.

Since 1992, he has been an Assistant Researcher with the Research Center of Inertial Navigation Equipment, HIT. From 1998 to 2004, he was an Associate Professor with HIT, where since 2004, he has been a Professor with the School of Electrical Engineering and Automation. His current research interests include high-power PMSG drives, integrated digital control for motors, and motor drive IP core-based FPGAs.